INITIAL STATE CHARACTERISTICS OF PROTON–NUCLEUS AND NUCLEUS–NUCLEUS COLLISIONS FROM GLAUBER MONTE CARLO

Maciej Rybczyński

Institute of Physics, Jan Kochanowski University, 25-406 Kielce, Poland
maciej.rybczynski@ujk.edu.pl

(Received September 12, 2013; revised version received November 19, 2013)

Fluctuations in physics observables in heavy-ion collisions have been a topic of particular interest in recent years as they may provide important signals regarding the formation of quark-gluon plasma and the existence of a critical point. We provide predictions for basic initial state characteristics of proton–nucleus and nucleus–nucleus collisions from Glauber Monte Carlo models. The following systems were simulated and analysed: p+^{12}C, p+^{14}N, p+^{63}Cu, p+^{208}Pb, ^{7}Be+^{9}Be, ^{40}Ar+^{40}Ca, ^{40}Ar+^{45}Sc, ^{63}Cu+^{63}Cu, ^{129}Xe+^{139}La and ^{208}Pb+^{208}Pb at wide energy range. We apply GLISSANDO accordingly fitted to tasks defined in this paper.

DOI:10.5506/APhysPolB.45.89
PACS numbers: 24.10.Lx, 24.60.Ky, 25.75.–q

1. Introduction

The relativistic nucleus–nucleus collisions have been studied over the last two decades. One of the main goals of these efforts is to understand the properties of strongly interacting matter under extreme conditions of very high energy, where the creation of the quark-gluon plasma (QGP) is expected [1, 2]. Various collision characteristics and their energy dependence suggest that a transient state of deconfined matter may be created at beam momentum as low as 30 A GeV/c [3], available at the CERN SPS. A detailed review of the experimental and theoretical status of the evidences for the onset of deconfinement gained by the NA49 Collaboration [4] at CERN SPS can be found in [5].

Fluctuations in physics observables in heavy-ion collisions have been a topic of particular interest in recent years as they may provide important signals regarding the formation of QGP and the existence of a critical point (CP). As an example, a significant transverse momentum and multiplicity fluctuations are expected to appear for systems freezing-out close to CP [6].

The above mentioned cogitations initiated an extensive program of fluctuation studies at the CERN SPS and BNL RHIC accelerators. Indeed, the NA49 Collaboration reported possible signals for critical point encoded in non-monotonic behavior of system size dependence of several hadronic observables [7–9]. Therefore, the efforts to look for CP will be continued within the NA61/SHINE [10] project, where the ultimate goal is to explore the phase diagram of strongly interacting matter in collisions of different systems from $p+p$, through $p+A$, to $A+A$ at projectile momenta of 13 A, 20 A, 30 A, 40 A, 80 A and 158 $A\,\mathrm{GeV}/c$. The energy scan of $p+p$ reactions was completed in 2009–2011. Data on $^{7}\mathrm{Be}+^{9}\mathrm{Be}$ collisions at three top energies were recorded in 2011, the remaining energies were taken in 2012. The energy scan of $p+^{208}\mathrm{Pb}$, $^{40}\mathrm{Ar}+^{40}\mathrm{Ca}$ and $^{129}\mathrm{Xe}+^{139}\mathrm{La}$ collisions is foreseen until 2016. In addition, a beam energy scan of $^{208}\mathrm{Pb}+^{208}\mathrm{Pb}$ collisions is planned.

The aim of this paper is to provide predictions for basic initial state characteristics of proton–nucleus and nucleus–nucleus collisions from Glauber Monte Carlo (GMC) models. To do this, we used GLISSANDO [11] accordingly fitted to tasks defined in this paper. The attention was paid for distributions of binary collisions as well as distributions of participants[1] from projectile and target. The fluctuations of number of target participants were also studied in few variants of GMC. In addition, an inelastic cross section, σ^{inel} was calculated for $^{7}\mathrm{Be}+^{9}\mathrm{Be}$ collisions at the SPS energy range and production cross section σ^{prod} for $p+^{14}\mathrm{N}$ interactions at the LHC energy. For later system, the range of σ^{prod} was estimated varying reasonable assumptions from GMC. This may be useful for cosmic ray physicists community, where the knowledge of σ^{prod} for proton–air interactions is crucial in proper simulations of the extensive air showers development in Earth's atmosphere.

The following systems were simulated and analysed: $p+^{12}\mathrm{C}$, $p+^{14}\mathrm{N}$, $p+^{63}\mathrm{Cu}$, $p+^{208}\mathrm{Pb}$, $^{7}\mathrm{Be}+^{9}\mathrm{Be}$, $^{40}\mathrm{Ar}+^{40}\mathrm{Ca}$, $^{40}\mathrm{Ar}+^{45}\mathrm{Sc}$, $^{63}\mathrm{Cu}+^{63}\mathrm{Cu}$, $^{129}\mathrm{Xe}+^{139}\mathrm{La}$ and $^{208}\mathrm{Pb}+^{208}\mathrm{Pb}$ at wide energy range from low SPS up to the LHC.

A brief description of the Glauber-like models is given in Section 2. In Section 3, a concise depiction of the Glauber Monte Carlo approach with particular attention to the model used in this work is provided. In Section 4, results of proton–nucleus simulation are presented and discussed, while Section 5 brings results for nucleus–nucleus collisions. Section 6 closes the article. In Appendix, we show distributions of target participants for given number of projectile participants in $^{7}\mathrm{Be}+^{9}\mathrm{Be}$ collisions and $p+^{208}\mathrm{Pb}$ interactions.

[1] In the present work, by the *participants* we call these nucleons which suffer at least *one* inelastic collision.

2. A brief description of Glauber-like models

The Glauber model [12] was formulated in late 1950s in order to find description of high-energy collision of atomic nuclei treated as composite structures. Until then, there was no systematic calculations regarding nuclear systems as projectile or target. Glauber model containing quantum theory of collisions of composite particles allows to describe experimental results on collisions of protons with deuterons and heavier nuclei. In the mid 1970s, Bialas *et al.* [13, 14] used Glauber model to describe inelastic nuclear collisions in their wounded-nucleon model. Bialas *et al.* [13] formulation allows to treat a collision between nuclei as a superposition of incoherent collisions between their nucleons. An excellent review of Glauber modeling of high-energy collisions was given in [15].

2.1. Nuclear charge densities

In the Glauber-like calculations some parameters must be provided from experiment. Usually, there are the nuclear charge densities and the energy dependence of the nucleon–nucleon cross section. In the Glauber model, the nucleons in nuclei are distributed randomly according to given nuclear density distribution. The radial nuclear density distribution, $\rho(r)$, determined from electron–nucleus scattering experiments is, for sufficiently heavy nuclei, usually in the Woods–Saxon type, modified to incorporate the shape of nuclei deformation [16–18]

$$\rho(r) = \frac{\rho_0}{1 + \exp\left(\frac{r - R(1+\beta_2 Y_{20} + \beta_4 Y_{40})}{a}\right)}, \tag{1}$$

where ρ_0 corresponds to the nucleon density in the center of nucleus, R corresponds to the nuclear radius, a to the skin depth, Y_{lm} are spherical harmonic functions of degree l and order m represented as a complex exponential and associated Legendre polynomials, and β_2 and β_4 are deformation parameters [19].

For heavy nuclei with atomic mass $A > 16$, the nuclear radii are well described by

$$R = \left(1.12\, A^{1/3} - 0.86\, A^{-1/3}\right)\ \text{fm}, \tag{2}$$

while $a = 0.54$ fm.

The nucleons are extended objects, so the centers of the nucleons cannot be closer than particular expulsion distance d — this is the usual way to introduce the nucleon–nucleon repulsion in GMC models. The magnitude of d should be proportional to the hard-core repulsion range in the nuclear potential. Since the repulsion implemented via the condition $d > 0$ increases (at the level of 1%), the size R of the nucleus then it should be compensated

by appropriate change of the distribution parameters used for generation of positions of nucleons centers. It was found in [20] that the following parametrization

$$\begin{aligned} R &= \left(1.1\,A^{1/3} - 0.656\,A^{-1/3}\right)\ \text{fm}\,, \\ a &= 0.459\ \text{fm} \end{aligned} \tag{3}$$

taken for $d = 0.9$ fm works well. Alvioli, Drescher and Strikman [21, 22] prepared distributions of nucleons in nuclei which contain the central two-body correlations between nucleons. The procedure was based on the Metropolis algorithm used for search for configurations satisfying limitations imposed by the nucleon–nucleon correlations. The one-body Woods–Saxon distribution as well as central nucleon–nucleon correlations, taken in the Gaussian form was reproduced. The effects of these correlations on heavy-ion observables turn out to be indistinguishable from the hard-core repulsion with $d = 0.9$ fm [20, 23]. In this paper, the nucleon expulsion distance $d = 0.9$ fm is used as a standard for all considered nuclei. Table I collects the values of Woods–Saxon parameters of heavy nuclei used in this work.

TABLE I

The Woods–Saxon parameters of heavy nuclei used in this work. The R values are taken from Eq. (3), while values of deformation parameters β_2 and β_4 — from [19].

Nucleus	R [fm]	β_2	β_4
^{40}Ar	3.57	0.0	0.0
^{40}Ca	3.57	0.0	0.0
^{45}Sc	3.728	0.0	0.0
^{63}Cu	4.212	0.162	−0.006
^{129}Xe	5.428	0.143	−0.001
^{139}La	5.571	0.0	0.0
^{208}Pb	6.407	0.0	0.0

For lighter nuclei, with mass number $3 \leq A \leq 16$ a harmonic oscillator shell model density is used [16, 17, 24]

$$\begin{aligned} \rho\,(r) &= \frac{4}{\pi^{3/2}C^3}\left[1 + \frac{A-4}{6}\left(\frac{r}{C}\right)^2\right]\exp\left(-r^2/C^2\right), \\ C^2 &= \left(\frac{5}{2} - \frac{4}{A}\right)^{-1}\left(\left\langle r^2_{\text{ch}}\right\rangle_A - \left\langle r^2_{\text{ch}}\right\rangle_p\right), \end{aligned} \tag{4}$$

where $\langle r^2_{\text{ch}}\rangle_A$ and $\langle r^2_{\text{ch}}\rangle_p = 0.7714$ fm^2 are the mean squared charge radii of the nucleus and proton, respectively [25]. The values of harmonic oscillator shell model parameter $\langle r^2_{\text{ch}}\rangle_A$ for light nuclei used in this work are shown in Table II.

TABLE II

The Harmonic oscillator shell model parameter $\langle r^2_{\rm ch}\rangle_A$ for several light nuclei [25]. The values include the case with no NN repulsion ($d = 0$) and with the repulsion implemented via expulsion radius of $d = 0.9$ fm and $d = 1.5$ fm.

Nucleus	$\langle r^2_{\rm ch}\rangle_A$ [fm^2]		
	$d = 0$	$d = 0.9$ fm	$d = 1.5$ fm
^{7}Be	7.00	6.69	5.66
^{9}Be	6.35	6.0	4.7
^{12}C	6.10	5.66	4.02
^{14}N	6.54	6.08	4.28

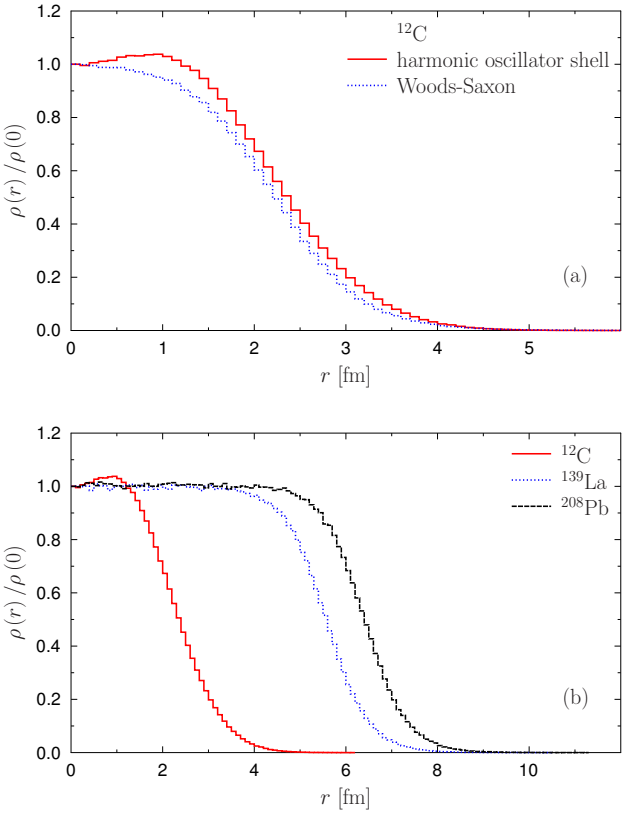

Fig. 1. Panel (a) — comparison between nuclear density distributions given by harmonic oscillator shell model and Woods–Saxon parametrization for ^{12}C nucleus. Panel (b) — nuclear density distributions for ^{12}C, ^{139}La and ^{208}Pb nuclei used in this paper.

The difference between nuclear density distributions given by harmonic oscillator shell model and Woods–Saxon parametrization for ^{12}C nucleus is shown in Fig. 1. There are also shown examples of the shapes of nuclear density distributions of ^{139}La and ^{208}Pb nuclei given by Woods–Saxon parametrization.

2.2. Cross sections

The multi-particle nucleon–nucleon processes are in the main interest of studying of high-energy nuclear collisions. Usually, the two types of processes are regarded — inelastic and production reactions. The production processes are those which lead to production of new hadrons. Among the inelastic processes, there are also interactions which result only in disintegration of the projectile or target nucleus (quasi-elastic interactions). The inelastic cross section $\sigma^{\rm inel}$ is the sum of the processes due to strong $p + A$ and $A + A$ interactions except the coherent nuclear elastic scattering. Thus, it contains interactions which result in production of new hadrons (production processes) and quasi-elastic interactions resulting in break up of the projectile or target nucleus. In high-energy experiments, the production cross section $\sigma^{\rm prod}$ is usually determined from the inelastic cross section by subtraction of the cross section of quasi-elastic $p+A$ and $A+A$ reactions [26].

The Glauber model was prepared for elastic collisions, where nucleon does not change its properties over individual collisions. Using of the Glauber model for inelastic collisions, it is assumed that after a single inelastic collision an excited nucleon-like object is created that interacts with the same nucleon–nucleon cross section with other nucleons [27].

In the present work, in order to simulate inelastic processes, the total collision proton–proton cross section, $\sigma^{\rm tot}_{NN}$ was used as an input. For the simulation of production processes, the total inelastic proton–proton cross section, $\sigma^{\rm inel}_{NN}$ was applied. This is the only way to introduce the beam energy dependence of Glauber calculations.

TABLE III

Total collision, $\sigma^{\rm tot}_{NN}$, and total inelastic, $\sigma^{\rm inel}_{NN}$, proton–proton cross sections for center-of-mass energies used in this work [28, 29]. $\sqrt{s_{NN}}$ is the center-of-mass energy for nucleon pair and $p_{\rm lab}$ is the beam momentum in the laboratory frame.

$\sqrt{s_{NN}}$ [GeV]	$p_{\rm lab}$ [GeV/c]	$\sigma^{\rm tot}_{NN}$ [mb]	$\sigma^{\rm inel}_{NN}$ [mb]
2.24	1.45	45.0	24.0
5.12	13.0	39.1	29.1
6.27	20.0	38.85	29.85
7.62	30.0	38.59	30.89
16.83	150.0	38.69	31.72
7 000.0	2.61×10^7	98.3	73.5

In the case of simulations at $\sqrt{s_{NN}} = 7\,000$ GeV, the values of proton–proton cross sections were taken from [28], while for all other energies — from the PDG library [29]. The total inelastic proton–proton cross section was calculated as a difference between total collision and total elastic proton–proton cross section. The values of proton–proton cross sections for center-of-mass energies used in this work are shown in Table III.

2.3. Nucleon–nucleon wounding profile

The nucleon–nucleon wounding profile (NNWP), $p(b)$, defined by the probability density $f(b)$ of inelastic nucleon–nucleon collision at the impact parameter b, plays a very important role in all Glauber like approaches and especially in wounding-nucleon model [13]. NNWP is normalized to the total inelastic nucleon–nucleon cross section

$$2\pi \int bp(b)\, db = \sigma_{NN}^{\text{inel}}\,. \tag{5}$$

Usually in Glauber Monte Carlo codes, it is assumed that $p(b)$ is given by the step function

$$p(b) = \Theta(R - b) \tag{6}$$

with $R = \sqrt{\sigma_{NN}^{\text{inel}}/\pi}$ and probability density distribution $f(b) = \frac{1}{R}\Theta(R-b)$. Later in the text, a profile function given by Eq. (6) we shall call a *hard-sphere* approximation.

The importance of the nucleon–nucleon wounding profile shape was discussed in [30, 31]. Following [32], where the CERN ISR experimental data for proton–proton differential cross section were properly parametrized with a combination of Gaussians, the profile function was proposed in the form [30]

$$p(b) = G \exp\left(-\frac{Gb^2}{R^2}\right) \tag{7}$$

with parameter $G = 0.92$. We shall call it a *Gaussian* approximation. In [31], there is a suggestion that cross section fluctuations given by the gamma distribution with relative variance $\omega = \text{Var}(\sigma)/\langle\sigma^2\rangle$, leads to the profile function

$$p(b) = \Gamma\left(\frac{1}{\omega}, \frac{b^2}{R^2\omega}\right) \Big/ \Gamma\left(\frac{1}{\omega}\right)\,, \tag{8}$$

where $\Gamma(z)$ is Euler gamma function, $\Gamma(\alpha, z)$ is incomplete gamma function, and parameter $\omega \in (0, 1)$. NNWP given by Eq. (8) — a *gamma* approximation — smoothly ranges between the both hard-sphere for $\omega \to 0$ and Gaussian, $\omega \to 1$ approximations.

In Fig. 2, the shapes of NNWP function $p\,(b)$ for hard-sphere, Gaussian and gamma approximations are shown. Gamma approximation with the parameter $\omega = 0.4$ corresponds to the shape of profile function which well reproduces the TOTEM data [33, 34] on elastic differential cross section measured in proton–proton interactions at $\sqrt{s_{NN}} = 7\,000$ GeV [31].

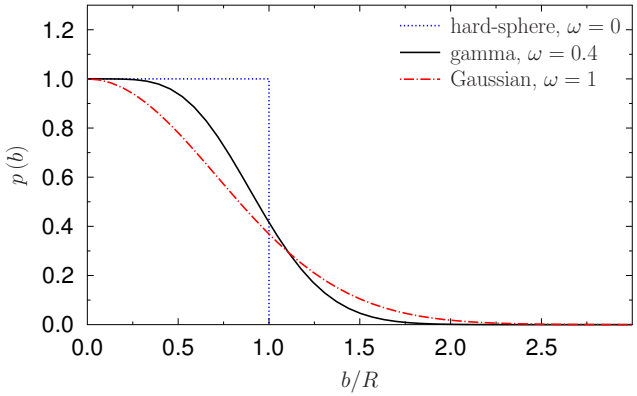

Fig. 2. Nucleon–nucleon wounding profile function $p\,(b)$ for hard-sphere, Gaussian and gamma approximations. Gamma approximation with parameter $\omega = 0.4$ [31] corresponds to the shape of profile function which well reproduces the TOTEM data [33, 34] on elastic differential cross section measured in proton–proton interactions at $\sqrt{s_{NN}} = 7\,000$ GeV.

3. GLISSANDO: The Glauber Monte Carlo approach

In the last few decades, the popular Glauber Monte Carlo approach started to be an essential tool in the analysis of relativistic heavy-ion collisions [15]. One of the most important application of the GMC simulation is the estimate of the number of participants dependence on the centrality, especially in the collider experiments [11, 15]. On the physics side, the presence of the event-by-event fluctuations in the initial Glauber phase is a crucial aspect of the approach. These geometric fluctuations are carried over to the final distributions of the experimentally measured hadrons. In many analyses, the Glauber-model initial state is used as an starting point for event-by-event hydrodynamics [35]. Among other aspects which are also considered with this approach, one can include the forward–backward correlations [36], the two-dimensional correlations in relative rapidity and azimuth [37], or jet quenching [38].

GLISSANDO [11] is a GMC generator for initial stages of relativistic heavy-ion collisions, written in C++ and interfaced to ROOT [39]. The program can be used for simulation of large variety of colliding systems:

$p + A$, $d + A$ and $A + A$ at wide spectrum of energies. Several models are implemented: the wounded-nucleon model [13][2], the binary collisions model, the mixed model [40, 41], and the model with hot-spots [42]. The program generates, among others, the variable-axes (participant) two- and three-dimensional profiles of the density of sources in the transverse plane and their Fourier components. These profiles can be used in further analyses of physics phenomena, such as the jet quenching, event-by-event hydrodynamics, or analysis of the elliptic flow and its fluctuations. Details can be found in [11].

The code of GLISSANDO published in [11] was slightly modified for the purposes defined in this work. Namely, a deformed Woods–Saxon nuclear density distribution with the deformation parameters, β_2 and β_4 was used for heavy nuclei (with mass number $A > 16$) and in the case of light nuclei (mass number $3 \leq A \leq 16$) — the harmonic oscillator shell model was applied.

4. Results for proton–nucleus interactions

In this section, results for some initial state characteristics of proton–nucleus interactions are described. Simulation of the production reactions of protons with ^{12}C, ^{14}N, ^{63}Cu and ^{208}Pb nuclei at three different center-of-mass energies, $\sqrt{s_{NN}} = 5.12$, 16.83 and 7 000 GeV was performed with few variants of wounded-nucleon model. Since the production processes are considered, thus the values of $\sigma_{NN}^{\text{inel}}$ are used. The results for $p + ^{208}$Pb system may be in particular interest of the NA61/SHINE Collaboration which recently collected data on $p + ^{208}$Pb interactions at CERN SPS energies.

In Fig. 3, the mean number of target participants $\langle N_p^{\text{targ}} \rangle$ as a function of target mass A is shown. There are results of GLISSANDO simulation within wounded-nucleon model with NNWP given by hard-sphere approximation. For reactions at all energies, a smooth increase of the average number of target participants with increasing mass of target nuclei is observed. In particular, at $\sqrt{s_{NN}} = 7\,000$ GeV it starts with $\langle N_p^{\text{targ}} \rangle \simeq 2.45$ for $p + ^{12}$C and ends with $\langle N_p^{\text{targ}} \rangle \simeq 7.61$ for $p + ^{208}$Pb interactions. For both lower energies, the increase of $\langle N_p^{\text{targ}} \rangle$ with mass number A is slower and similar to each other.

The target mass dependence of $\langle N_p^{\text{targ}} \rangle$ may be described by simple power-law formula

$$\langle N_p^{\text{targ}} \rangle = N_0 \, A^{\alpha} \,, \tag{9}$$

with parameters N_0 and α given in Table IV. The α exponent slightly increases its value from $\alpha \simeq 0.3$ at $\sqrt{s_{NN}} = 5.12$ GeV up to $\alpha \simeq 0.4$ for the LHC energy, $\sqrt{s_{NN}} = 7\,000$ GeV.

[2] In this paper, for simplicity, we focus on the results from wounded-nucleon model applied with few variants of nucleon–nucleon wounding profile.

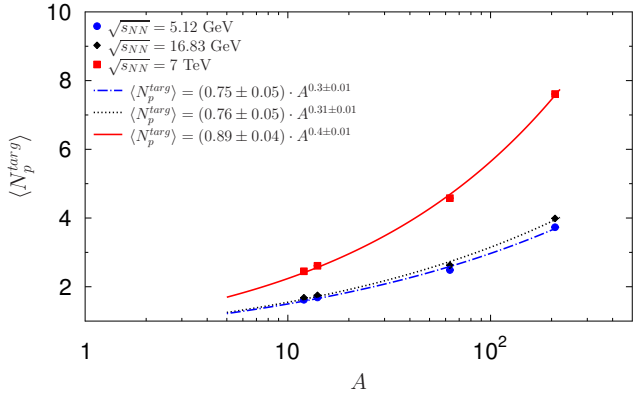

Fig. 3. The mean number of target participants $\langle N_p^{\mathrm{targ}}\rangle$ as a function of target mass A. The results of GLISSANDO simulation for production reactions of protons with ^{12}C, ^{14}N, ^{63}Cu and ^{208}Pb ions at $\sqrt{s_{NN}} = 5.12$, 16.83 and 7 000 GeV. The wounded-nucleon model with NNWP given by the hard-sphere approximation fitted by Eq. (9).

TABLE IV

Parameters used in Eq. (9).

$\sqrt{s_{NN}}$ [GeV]	N_0	α
5.12	0.75 ± 0.05	0.3 ± 0.01
16.83	0.76 ± 0.05	0.31 ± 0.01
7 000.0	0.89 ± 0.04	0.4 ± 0.01

The resultant fluctuations of the number of target participants as a function of target atomic mass A are presented in Fig. 4. Again, wounded-nucleon model with NNWP given by hard-sphere approximation was applied. As a measure of these fluctuations, we used the scaled variance of the distribution of target participants number

$$\omega_p^{\mathrm{targ}} = \frac{\mathrm{Var}\left(N_p^{\mathrm{targ}}\right)}{\left\langle N_p^{\mathrm{targ}}\right\rangle}, \tag{10}$$

where $\mathrm{Var}\left(N_p^{\mathrm{targ}}\right)$ describes variance of the number of target participants and $\langle N_p^{\mathrm{targ}}\rangle$ its mean value.

For SPS energies, $\sqrt{s_{NN}} = 5.12$, 16.83 GeV, the value of ω_p^{targ} is of the order of unity for $p + {}^{63}$Cu interactions, what corresponds to the number of target participants given by the Poisson distribution. For $p + {}^{12}$C and

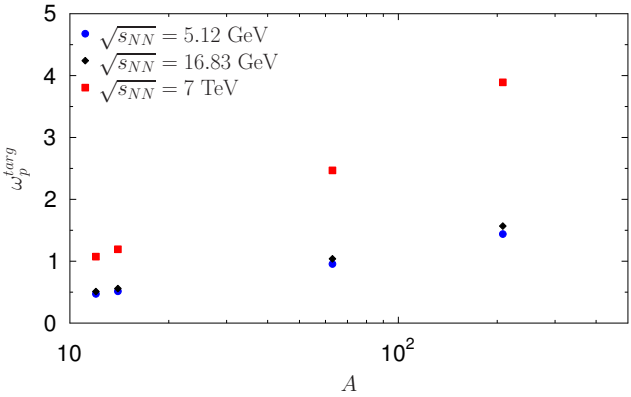

Fig. 4. Scaled variance of the distribution of target participants number, ω_p^{targ} as a function of target atomic mass A. The results of GLISSANDO simulation for production reactions of protons with ^{12}C, ^{14}N, ^{63}Cu and ^{208}Pb ions at $\sqrt{s_{NN}}$ = 5.12, 16.83 and 7 000 GeV. The wounded-nucleon model with NNWP given by the hard-sphere approximation.

$p + {}^{14}$N reactions, ω_p^{targ} has significantly lower values than one, whereas for $p + {}^{208}$Pb reactions — slightly higher. For LHC energy, $\sqrt{s_{NN}} = 7\,000$ GeV the value of ω_p^{targ} starts with around one for $p + {}^{12}$C and ends with $\omega_p^{\mathrm{targ}} \simeq 4$ for $p + {}^{208}$Pb interactions.

The comparison of ω_p^{targ} values obtained for $p + {}^{208}$Pb production reactions simulated with different shapes of NNWP, namely hard-sphere, Gaussian and gamma approximations is shown in Fig. 5. For the LHC energy, $\sqrt{s_{NN}} = 7\,000$ GeV besides of hard-sphere and Gaussian — the NNWP given by gamma approximation with parameter $\omega = 0.4$ [31] was used. There is a small difference between hard-sphere and Gaussian approximations, of the order of few percents, however Gaussian approximation leads to higher fluctuations of target participants for all considered energies. Gamma approximation for the LHC energy gives fluctuations of the number of target participants just in the middle between above mentioned hard-sphere and Gaussian.

Let us finish this section with some predictions which may be interesting for cosmic ray physicists community. In the modeling of propagation of cosmic rays through atmosphere, a knowledge of production proton–air cross section, $\sigma^{\mathrm{prod}}_{p+\mathrm{air}}$ plays a very important role. As air is mainly composed with ^{14}N nuclei, we simulated $p+{}^{14}$N production reactions at $\sqrt{s_{NN}} = 7\,000$ GeV. In order to estimate the possible range of $\sigma^{\mathrm{prod}}_{p+\mathrm{N}}$, we performed simulations with all: hard-sphere, Gaussian and gamma with parameter $\omega = 0.4$ nucleon–nucleon wounding profiles. Besides, we also varied the value of

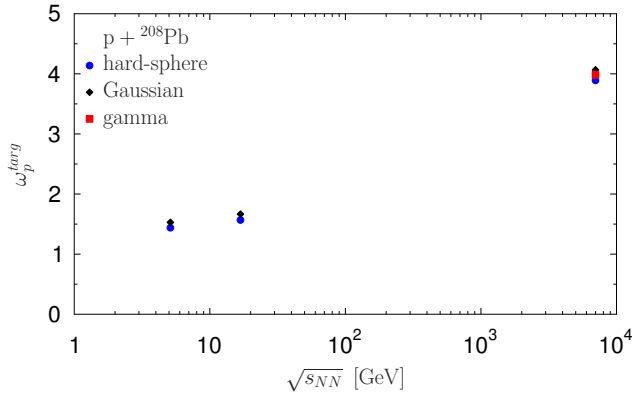

Fig. 5. Scaled variance of the target participant number distribution as a function of center-of-mass energy. The comparison of results of GLISSANDO simulation for $p + {}^{208}\mathrm{Pb}$ production reactions. The wounded-nucleon model with NNWP given by hard-sphere, Gaussian and gamma with parameter $\omega = 0.4$ approximations.

nucleon expulsion distance d. In Table V, we put the obtained values of $\sigma^{\mathrm{prod}}_{p+\mathrm{N}}$. As the proton–proton total inelastic cross section at the LHC energy is known with the uncertainty $\sigma^{\mathrm{inel}}_{NN} = 73.5^{+1.8}_{-1.3}$ mb [28], we simulated $p+{}^{14}\mathrm{N}$ interactions with three different values of $\sigma^{\mathrm{inel}}_{NN} = 73.5$, 75.3 and 72.2 mb for standard, upper and lower limit. The corresponding uncertainty estimates are shown in Table V as positive and negative numbers next to the evaluated values of $\sigma^{\mathrm{prod}}_{p+\mathrm{N}}$.

TABLE V

Production cross section, $\sigma^{\mathrm{prod}}_{p+\mathrm{N}}$ for $p + {}^{14}\mathrm{N}$ interactions at $\sqrt{s_{NN}} = 7\,000$ GeV. Simulation performed with total inelastic proton–proton cross section $\sigma^{\mathrm{inel}}_{NN} = 73.5^{+1.8}_{-1.3}$ mb [28]. The upper (positive) uncertainty comes from simulations with $\sigma^{\mathrm{inel}}_{NN} = 75.3$ mb, while the lower one — from $\sigma^{\mathrm{inel}}_{NN} = 72.2$ mb.

d [fm]	$\sigma^{\mathrm{prod}}_{p+\mathrm{N}}$ [mb] (hard-sphere)	$\sigma^{\mathrm{prod}}_{p+\mathrm{N}}$ [mb] (gamma)	$\sigma^{\mathrm{prod}}_{p+\mathrm{N}}$ [mb] (Gaussian)
0	$391.5^{+5.1}_{-3.7}$	$413.7^{+5.6}_{-4.2}$	$451.7^{+7.5}_{-5.1}$
0.9	$394.3^{+5.1}_{-3.3}$	$415.1^{+6.0}_{-4.1}$	$452.4^{+7.4}_{-5.5}$
1.5	$396.7^{+4.9}_{-3.4}$	$416.3^{+5.9}_{-3.6}$	$452.3^{+6.9}_{-5.3}$

Recently, the NA61/SHINE Collaboration measured production and inelastic cross section for $p + {}^{12}\mathrm{C}$ interactions at beam momentum $p_{\mathrm{lab}} = 31$ GeV/c [26]. The measured values are $\sigma^{\mathrm{prod}}_{p+\mathrm{C}} = 229.3 \pm 9$ mb and $\sigma^{\mathrm{inel}}_{p+\mathrm{C}} = 257.2 \pm 8.9$ mb, respectively. Our simulation for $p + {}^{12}\mathrm{C}$ interactions with

NNWP given by hard-sphere approximation and nucleon–nucleon expulsion distance $d = 0.9$ results with the production cross section $\sigma^{\text{prod}}_{p+\text{C}} = 222.9$ mb[3], and $\sigma^{\text{inel}}_{p+\text{C}} = 253.4$ mb, respectively, what is in good agreement with NA61/SHINE data. This fact, together with the one stated in Section 2, leads us to use NNWP given by hard-sphere approximation with nucleon–nucleon expulsion distance $d = 0.9$ as standard. Thus, $\sigma^{\text{prod}}_{p+\text{N}} = 394.3^{+5.1}_{-3.3}$ mb should be used as a reference point for $p + {}^{14}\text{N}$ production cross section at $\sqrt{s_{NN}} = 7\,000$ GeV. However, as other parametrisations also look reasonable, then larger variation of $\sigma^{\text{prod}}_{p+\text{N}} \in (390, 460)$ mb may be measured experimentally.

In Fig. 6, we present proton–nucleus production cross section $\sigma^{\text{prod}}_{p+A}$ as a function of target mass A. As in the case of average number of target, participants dependence on target mass and following [43], we use the power-law function

$$\sigma^{\text{prod}}_{p+A} = \sigma_0 \, A^{\gamma} \tag{11}$$

with parameters σ_0 and γ given in Table VI to fit the simulated values of $\sigma^{\text{prod}}_{p+A}$. Here, γ exponent slightly decrease its value from $\gamma \simeq 0.68$ at $\sqrt{s_{NN}} = 5.12$ GeV to $\gamma \simeq 0.59$ for $\sqrt{s_{NN}} = 7\,000$ GeV.

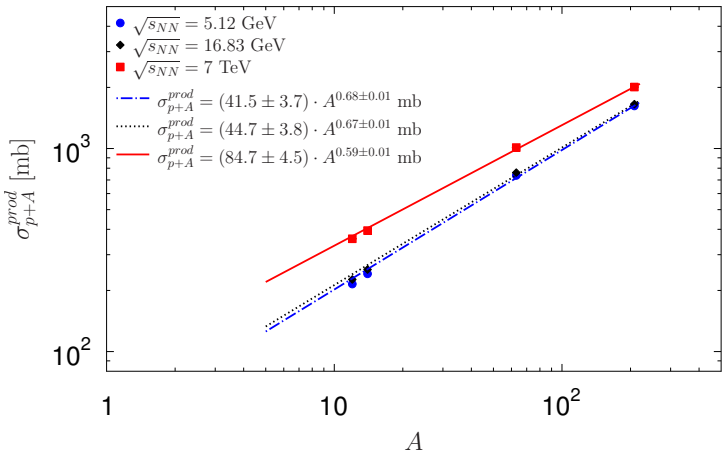

Fig. 6. Proton–nucleus production cross section $\sigma^{\text{prod}}_{p+A}$ as a function of target mass A. The results of the GLISSANDO simulation for production reactions of protons with ${}^{12}\text{C}$, ${}^{14}\text{N}$, ${}^{63}\text{Cu}$ and ${}^{208}\text{Pb}$ ions at $\sqrt{s_{NN}} = 5.12$, 16.83 and 7 000 GeV. The wounded-nucleon model with NNWP given by the hard-sphere approximation fitted by Eq. (11).

[3] For NNWP given by hard-sphere approximation with $d = 0$ and $d = 1.5$ fm, the values of $\sigma^{\text{prod}}_{p+\text{C}}$ for $p + {}^{12}\text{C}$ interactions are 217.4 and 232.5 mb, respectively.

TABLE VI

Parameters used in Eq. (11).

$\sqrt{s_{NN}}$ [GeV]	σ_0 [mb]	γ
5.12	41.5 ± 3.7	0.68 ± 0.01
16.83	44.7 ± 3.8	0.67 ± 0.01
7 000.0	84.7 ± 4.5	0.59 ± 0.01

It may be interesting to look how the production cross section $\sigma^{\rm prod}_{p+{\rm N}}$ simulated in high-energy $p + {}^{14}{\rm N}$ interactions depends on the total inelastic proton–proton cross section $\sigma^{\rm inel}_{NN}$. The according simulation was performed and the results are shown in Fig. 7[4]. There is a difference between two extreme cases given by hard-sphere and Gaussian nucleon–nucleon wounding profiles; namely Gaussian wounding profile leads to the faster growth of $\sigma^{\rm prod}_{p+{\rm N}}$ with $\sigma^{\rm inel}_{NN}$. The power-law fits to the simulated points result in:

$$\sigma^{\rm prod,\,hard-sphere}_{p+{\rm N}} = (40.61 \pm 0.12) \left(\sigma^{\rm inel}_{NN}\right)^{0.53\pm0.0007} \text{ mb}\,, \tag{12}$$

and

$$\sigma^{\rm prod,\,Gaussian}_{p+{\rm N}} = (26.56 \pm 0.72) \left(\sigma^{\rm inel}_{NN}\right)^{0.66\pm0.006} \text{ mb}\,, \tag{13}$$

for hard-sphere and Gaussian wounding profiles, respectively.

In Ref. [44], the Pierre Auger Collaboration calculated proton–air production cross section, $\sigma^{\rm prod}_{p+{\rm air}}$ at $\sqrt{s_{NN}} = 57$ TeV from cosmic ray data, to be equal $\sigma^{\rm prod}_{p+{\rm air}} = 505^{+28}_{-36}$ mb. There was also found the corresponding inelastic proton–proton cross section, $\sigma^{\rm inel}_{NN} = 92^{+9}_{-11}$ mb. From our fits, Eqs. (12)–(13) to $p + {}^{14}{\rm N}$ GLISSANDO simulation, we found $\sigma^{\rm prod,\,hard-sphere}_{p+{\rm N}}(92 \text{ mb}) \simeq 446$ mb and $\sigma^{\rm prod,\,Gaussian}_{p+{\rm N}}(92 \text{ mb}) \simeq 525$ mb what determines the limits for $p + {}^{14}{\rm N}$ production cross section at $\sqrt{s_{NN}} = 57$ TeV and is in quite good agreement with [44].

From the other side, with the use of Eqs. (12)–(13) it is possible to estimate the possible ranges of $\sigma^{\rm inel}_{NN}$ at $\sqrt{s_{NN}} = 57$ TeV. We recovered the Pierre Auger Collaboration $\sigma^{\rm prod}_{p+{\rm N}} = 505$ mb [44] at $\sigma^{\rm inel}_{NN} \simeq 87$ mb (Gaussian approximation) and $\sigma^{\rm inel}_{NN} \simeq 116$ mb (hard-sphere approximation).

[4] In order to obtain the presented result, the five different values of the total inelastic proton–proton cross section was chosen corresponding to center-of-mass energies $\sqrt{s_{NN}}$ equal to 5.12, 6.27, 7.62, 16.83 and 7 000 GeV. We performed also a simulation for $\sigma^{\rm inel}_{NN} = 150$ mb corresponds to energies available in cosmic ray physics.

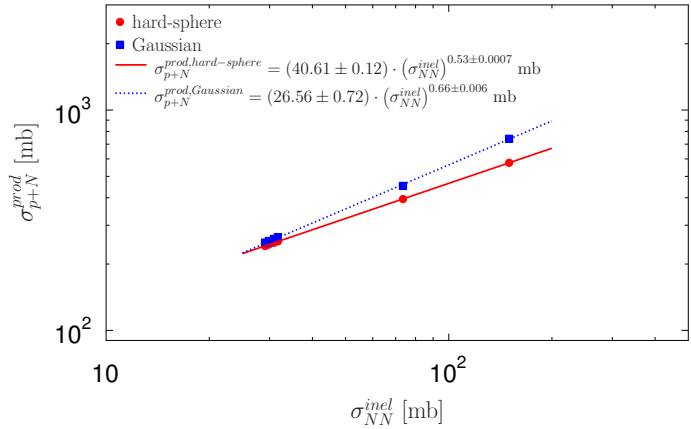

Fig. 7. $p + {}^{14}\mathrm{N}$ production cross section, $\sigma_{p+\mathrm{N}}^{\mathrm{prod}}$ as a function of total inelastic proton–proton cross section, $\sigma_{NN}^{\mathrm{inel}}$. Simulation for the wounded-nucleon model with hard-sphere and Gaussian nucleon–nucleon wounding profiles, both with expulsion distance $d = 0.9$ fm. See the text for details.

5. Results for nucleus–nucleus collisions

In this section, we describe results for some initial state characteristics of nucleus–nucleus collisions. The following systems were simulated and analysed: ${}^{7}\mathrm{Be} + {}^{9}\mathrm{Be}$, ${}^{40}\mathrm{Ar} + {}^{40}\mathrm{Ca}$, ${}^{40}\mathrm{Ar} + {}^{45}\mathrm{Sc}$, ${}^{63}\mathrm{Cu} + {}^{63}\mathrm{Cu}$, ${}^{129}\mathrm{Xe} + {}^{139}\mathrm{La}$ and ${}^{208}\mathrm{Pb} + {}^{208}\mathrm{Pb}$ at three different center-of-mass energies, $\sqrt{s_{NN}} = 5.12$, 16.83 and 7 000 GeV. Particular attention was paid to estimate the inelastic cross section, $\sigma_{\mathrm{Be+Be}}^{\mathrm{inel}}$ for ${}^{7}\mathrm{Be} + {}^{9}\mathrm{Be}$ collisions which is in the special interest of NA61/SHINE Collaboration due to experimental data taken for these reactions recently. Thus, in the case of ${}^{7}\mathrm{Be}+{}^{9}\mathrm{Be}$ collisions, the corresponding simulation was performed for additional energies.

In Fig. 8, the probability distributions, $P\left(N_p^{\mathrm{proj}}\right)$ of the number of projectile participants scaled by the projectile nucleus mass number, A^{proj} are shown. There are results of GLISSANDO simulation for production reactions of analysed ions at $\sqrt{s_{NN}} = 5.12$, 16.83 and 7 000 GeV within wounded-nucleon model with wounding profile given by hard-sphere approximation. Shapes of considered distributions are similar for most systems while scaled by A^{proj}. Only in the case of collisions of the lightest, ${}^{7}\mathrm{Be} + {}^{9}\mathrm{Be}$ system at SPS energies $\sqrt{s_{NN}} = 5.12$ and 16.83 GeV, there are slight differences, possibly due to small mass of beryllium nuclei.

In Fig. 9, a ratio of the mean number of target participants $\langle N_p^{\mathrm{targ}} \rangle$ to projectile participants N_p^{proj} as a function of $N_p^{\mathrm{proj}}/A^{\mathrm{proj}}$ is plotted. Again, the production reactions were simulated and the wounded-nucleon model

with wounding profile given by hard-sphere approximation was used. The plotted ratio is slightly above unity for peripheral collisions while for central collisions starts to be below one.

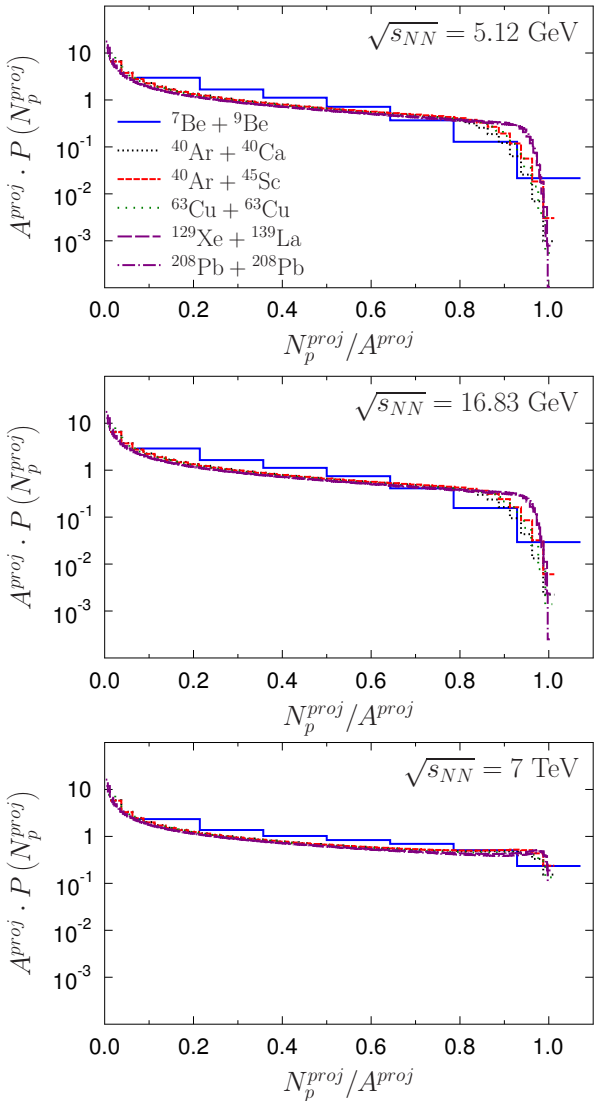

Fig. 8. Probability distribution of the number of projectile participants, $P\left(N_p^{\mathrm{proj}}\right)$ scaled by the projectile nucleus mass number, A^{proj}. The results of GLISSANDO simulation for production reactions of considered ions at $\sqrt{s_{NN}} = 5.12$ — top panel, 16.83 — middle panel and 7 000 GeV — bottom panel. The wounded-nucleon model with wounding profile given by the hard-sphere approximation.

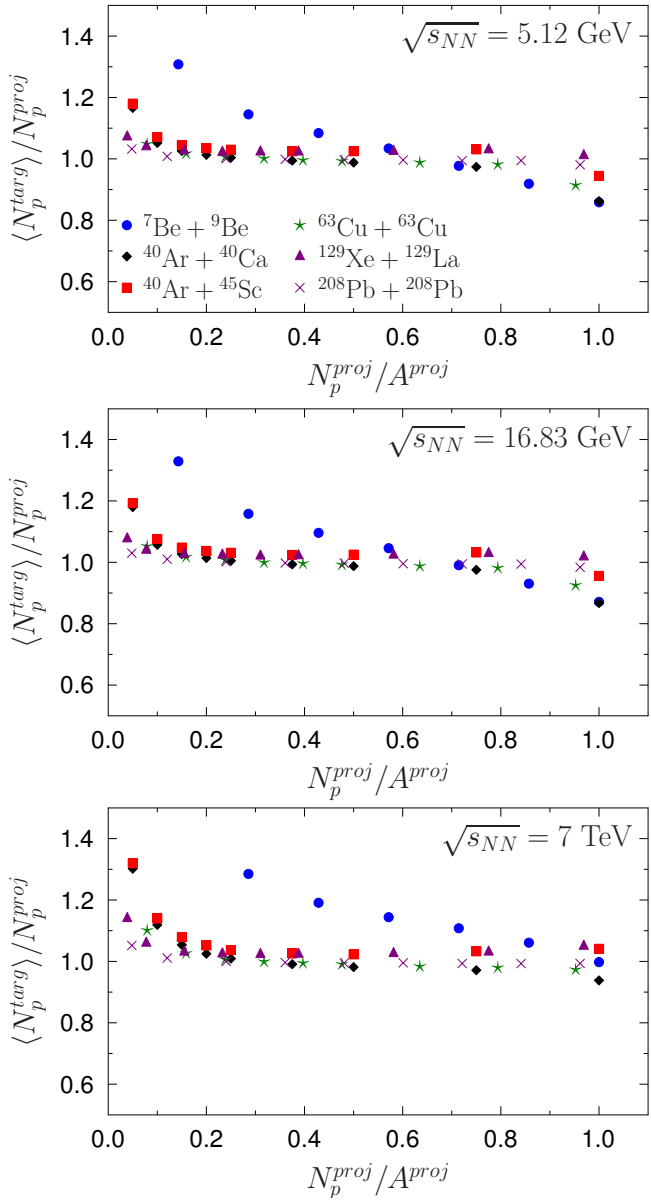

Fig. 9. Ratio of the mean number of target participants $\langle N_p^{\mathrm{targ}} \rangle$ to projectile participants N_p^{proj} as a function of $N_p^{\mathrm{proj}}/A^{\mathrm{proj}}$. The results of GLISSANDO simulation for production reactions of considered ions at $\sqrt{s_{NN}} = 5.12$ — top panel, 16.83 — middle panel and 7 000 GeV — bottom panel. The wounded-nucleon model with wounding profile given by the hard-sphere approximation.

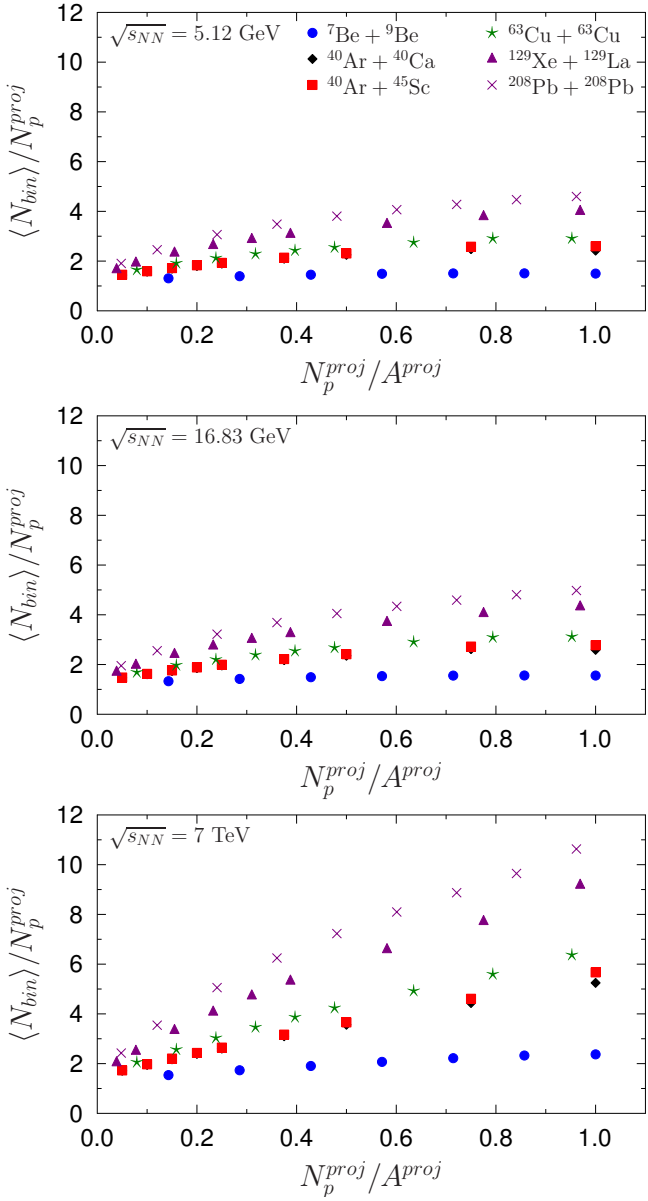

Fig. 10. The mean number of binary collisions, $\langle N_{\rm bin} \rangle$ scaled by the number of projectile participants $N_p^{\rm proj}$ as a function of $N_p^{\rm proj}/A^{\rm proj}$. The results of GLISSANDO simulation for production reactions of considered ions at $\sqrt{s_{NN}} = 5.12$ — top panel, 16.83 — middle panel and 7 000 GeV — bottom panel. The wounded-nucleon model with wounding profile given by the hard-sphere approximation.

In the case of binary collisions, the observation is opposite. In Fig. 10, where we plot the mean number of binary collisions, $\langle N_{\rm bin}\rangle$ scaled by the number projectile participants $N_p^{\rm proj}$ as a function of $N_p^{\rm proj}/A^{\rm proj}$, the smallest value is for peripheral collision for all considered systems and energies, and monotonically grows when going to more central collisions. The highest value is observed, as expected, for ^{208}Pb+^{208}Pb collisions at the LHC energy.

Following particular interest of the NA61/SHINE Collaboration with fluctuations/correlations studies in search for the critical point, we plot the scaled variance of distribution of the number of target participants, given by Eq. (10), as a function of $N_p^{\rm proj}/A^{\rm proj}$. There is a non-monotonic behavior of $\omega_p^{\rm targ}$ with maximum located in peripheral collisions for all simulated systems at all considered energies, see Fig. 11. The results, as expected, indicate the highest fluctuations for the heaviest system, ^{208}Pb + ^{208}Pb, with maximum equal 1.6, 1.7, and 2.7 for $\sqrt{s_{NN}} = 5.12$, 16.83 and 7 000 GeV, respectively. Similar analysis was done by Konchakovski *et al.* [45]. The important message for the fixed target experiments (*i.e.* NA61/SHINE) is that in order to reduce the possible influence of target participants fluctuations on measured quantities like multiplicity or transverse momentum fluctuations, they should either record as central (large $N_p^{\rm proj}$) collisions as possible or focus in the analysis on the results which comes from the projectile hemisphere[5], where such influence is, presumably, limited.

It may be interesting to check the influence of the shape of the wounding profile for the fluctuations of number of target participants. For that purpose, we selected medium system — ^{40}Ar + ^{45}Sc and plotted $\omega_p^{\rm targ}$ as a function of $N_p^{\rm proj}/A^{\rm proj}$ for three described above wounding profiles, see Fig. 12. The highest fluctuations are observed for the hard-sphere wounding profile at all energies — this is opposite to the case of p+A interactions where the highest values appeared for the Gaussian approximation. This may be understood as fluctuations in the number of target participants originate both from cross section fluctuations and from fluctuations of the number of nucleons along the path of projectile [31].

As in previous section, we finish with the Glauber Monte Carlo prediction for cross sections. Since NA61/SHINE measured *inelastic* ^{7}Be + ^{9}Be cross sections, $\sigma^{\rm inel}_{\rm Be+Be}$ [46], we performed simulation of ^{7}Be + ^{9}Be reactions with the use of total collision proton–proton cross sections, $\sigma^{\rm tot}_{NN}$ as given in Table III. In Fig. 13, GLISSANDO results were obtained with nucleon–nucleon wounding profile given by hard-sphere approximation with nucleon–nucleon expulsion distance $d = 0.9$ fm. GLISSANDO predictions are consistent with the measured NA61/SHINE [46] inelastic cross sections. As a low energy reference point, we used the inelastic ^{7}Be + ^{9}Be cross section measured at BEVALAC for $\sqrt{s_{NN}} = 2.24$ GeV [47].

[5] Particles are produced in the projectile hemisphere if their center of mass rapidities, y fulfill the condition $y > 0$.

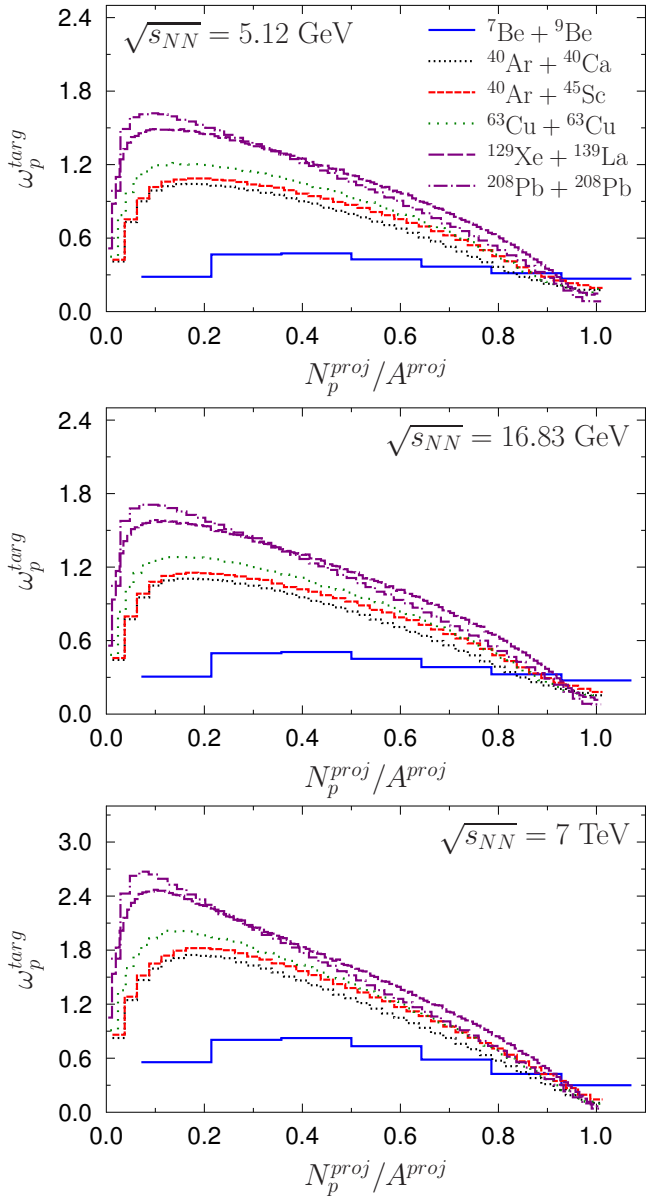

Fig. 11. Scaled variance of the target participant number distribution as a function of $N_p^{\mathrm{proj}}/A^{\mathrm{proj}}$. The results of GLISSANDO simulation for production reactions of considered ions at $\sqrt{s_{NN}} = 5.12$ — top panel, 16.83 — middle panel and 7 000 GeV — bottom panel. The wounded-nucleon model with wounding profile given by the hard-sphere approximation.

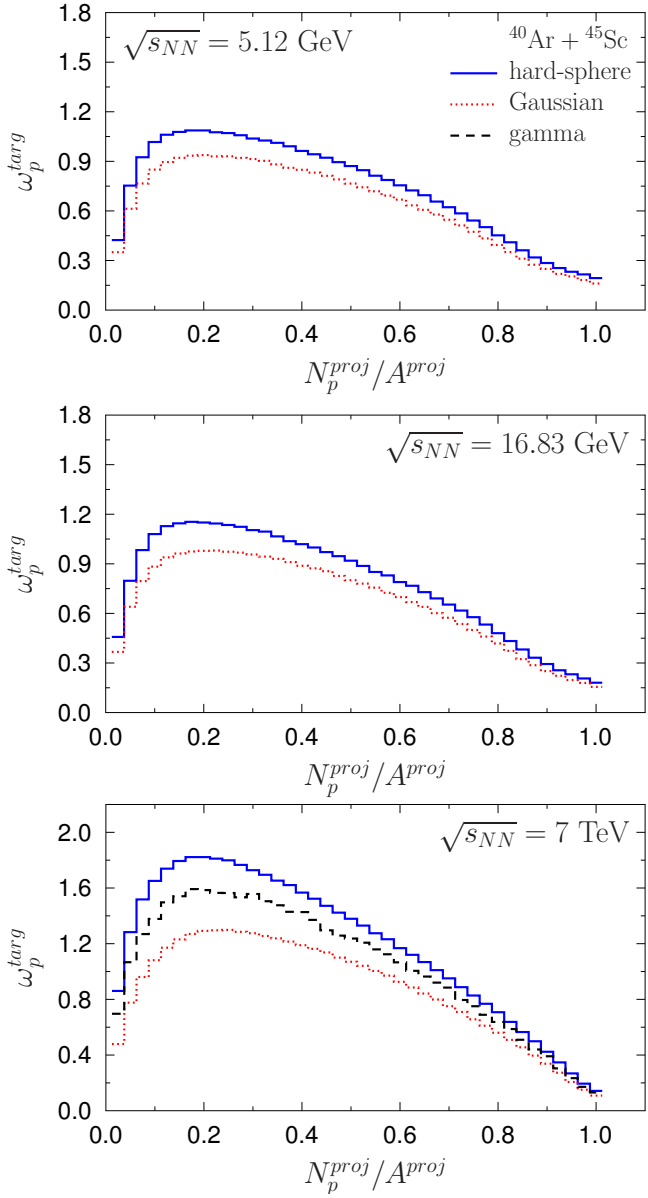

Fig. 12. Scaled variance of distribution of the number of target participants as a function of $N_p^{\mathrm{proj}}/A^{\mathrm{proj}}$. The comparison of results of GLISSANDO simulation for ^{40}Ar + ^{45}Sc production reactions at $\sqrt{s_{NN}} = 5.12$, 16.83 and 7 000 GeV. The wounded-nucleon model with wounding profile given by hard-sphere, Gaussian, and gamma approximations.

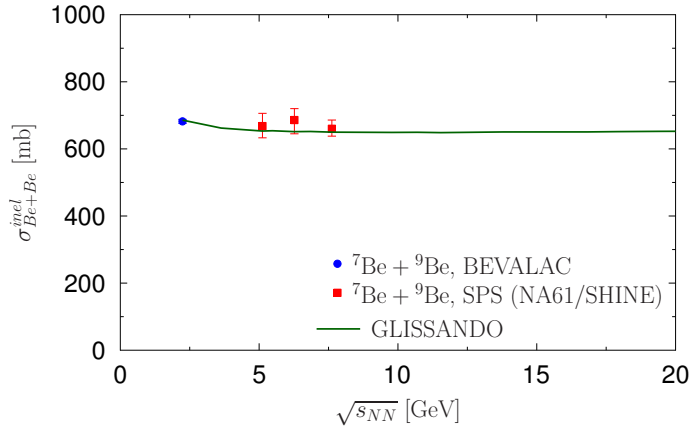

Fig. 13. Inelastic cross section, $\sigma^{\text{inel}}_{\text{Be+Be}}$ for ^{7}Be + ^{9}Be inelastic collisions. Results from BEVALAC [47] (blue circle) and SPS (NA61/SHINE) [46] (red squares) are compared with predictions of GLISSANDO. See the text for details.

6. Summary

The initial state characteristics of proton–nucleus and nucleus–nucleus collisions were simulated and analysed with the use of Glauber Monte Carlo code GLISSANDO. The following systems were studied: $p + {}^{12}$C, $p + {}^{14}$N, $p + {}^{63}$Cu, $p + {}^{208}$Pb, ^{7}Be + ^{9}Be, ^{40}Ar + ^{40}Ca, ^{40}Ar + ^{45}Sc, ^{63}Cu + ^{63}Cu, ^{129}Xe + ^{139}La and ^{208}Pb + ^{208}Pb at a wide energy range from low SPS up to LHC. Our main results are as follows:

In the case of proton–nucleus interactions:

- The mean number of target participants as a function of atomic mas of target nucleus was plotted and discussed. A simple power-law fit with the exponent around 1/3 was found to properly describe the above dependence for SPS as well as LHC energies. The value of this exponent slightly *increases* with the increasing energy of collision.

- Fluctuations of target participants described by scaled variance of target participants distributions were plotted as a function of target nucleus mass and collision center-of-mass energy. An influence of wounding profile on scaled variance was discussed.

- Production cross section as a function of target mass was estimated and fitted by power-law formula with the exponent around 2/3. The value of the exponent slightly *decreases* with the increasing energy of collision.

- For p+^{14}N interactions, the production cross section, $\sigma^{\mathrm{prod}}_{p+\mathrm{N}}$ at $\sqrt{s_{NN}} =$ 7 TeV was estimated to be equal $\sigma^{\mathrm{prod}}_{p+\mathrm{N}} = 394.3^{+5.1}_{-3.3}$ mb. Additionally, the dependence of $\sigma^{\mathrm{prod}}_{p+\mathrm{N}}$ on total inelastic proton–proton cross section was found and described by power-law functions for hard-sphere and Gaussian nucleon–nucleon wounding profiles.

- With the use of above mentioned formulas, the range of production $p + {}^{14}$N cross section ($\sigma^{\mathrm{prod}}_{p+\mathrm{N}} \in (446, 525)$ mb) as well as range of total inelastic proton–proton cross section ($\sigma^{\mathrm{inel}}_{NN} \in (87, 116)$ mb) at $\sqrt{s_{NN}} =$ 57 TeV was estimated.

In the case of nucleus–nucleus collisions:

- Probability distributions of the number of projectile participants was plotted and discussed. A similar shape of considered distributions was found when scaled by projectile nucleus atomic mass number, A^{proj}.

- A ratio of the mean number of target participants $\langle N_p^{\mathrm{targ}} \rangle$ to projectile participants N_p^{proj} was found to be decreasing function of $N_p^{\mathrm{proj}}/A^{\mathrm{proj}}$, similar for all considered systems.

- The mean number of binary collisions, $\langle N_{\mathrm{bin}} \rangle$ scaled by the number projectile participants N_p^{proj} is an increasing function of $N_p^{\mathrm{proj}}/A^{\mathrm{proj}}$, the smallest value is for peripheral collision for all considered systems and energies and monotonically grows when going to more central collisions.

- The scaled variance of the number of target participants distribution plotted as a function of $N_p^{\mathrm{proj}}/A^{\mathrm{proj}}$ shows a non-monotonic behavior with maximum located in peripheral collisions for all simulated systems at all considered energies. The results, as expected, indicate the highest fluctuations for the heaviest system, $^{208}\mathrm{Pb} + {}^{208}\mathrm{Pb}$, with maximum equal 1.6, 1.7, and 2.7 for $\sqrt{s_{NN}} = 5.12$, 16.83 and 7 000 GeV, respectively.

- The influence of the shape of the wounding profile for the fluctuations of number of target participants was checked. The highest fluctuations are observed for hard-sphere wounding profile at all energies — this is opposite to the case of $p + A$ interactions where the highest values appeared for Gaussian approximation.

- The GLISSANDO prediction for the inelastic ^{7}Be + ^{9}Be cross sections, $\sigma^{\rm inel}_{\rm Be+Be}$, was made and good agreement with the preliminary NA61/SHINE results was found when nucleon–nucleon wounding profile given by hard-sphere approximation with nucleon–nucleon expulsion distance $d = 0.9$ fm was used.

I am grateful to Zbigniew Włodarczyk and Marek Gaździcki for their very useful comments and suggestions. This work was supported by the National Science Centre grants DEC-2011/01/D/ST2/00772 and DEC-2012/04/M/ST2/00816.

7. Appendix

In Figs. 14 and 15, we show distributions of target participants for given number of projectile participants in ^{7}Be + ^{9}Be and p + ^{208}Pb reactions at $\sqrt{s_{NN}} = 16.83$ GeV. The mean number of target participants $\langle N_p^{\rm targ}\rangle$ and variance of number of target participants distribution Var $\left(\mathrm{N_p^{targ}}\right)$ for $p + {}^{208}$Pb production reactions are 3.989 ± 0.0008 and 6.255 ± 0.002, respectively. The corresponding moments of distributions of target participants in ^{7}Be + ^{9}Be production reactions are presented in Table VII.

TABLE VII

Mean values and variances of distributions of target participants in ^{7}Be + ^{9}Be production reactions plotted in Fig. 14.

$N_p^{\rm proj}$	$\langle N_p^{\rm targ}\rangle$	Var $\left(N_p^{\rm targ}\right)$
1	1.329 ± 0.0003	0.4063 ± 0.0002
2	2.316 ± 0.0007	1.1513 ± 0.0007
3	3.287 ± 0.001	1.6667 ± 0.001
4	4.182 ± 0.001	1.888 ± 0.002
5	4.953 ± 0.002	1.899 ± 0.002
6	5.583 ± 0.003	1.812 ± 0.004
7	6.098 ± 0.007	1.677 ± 0.009

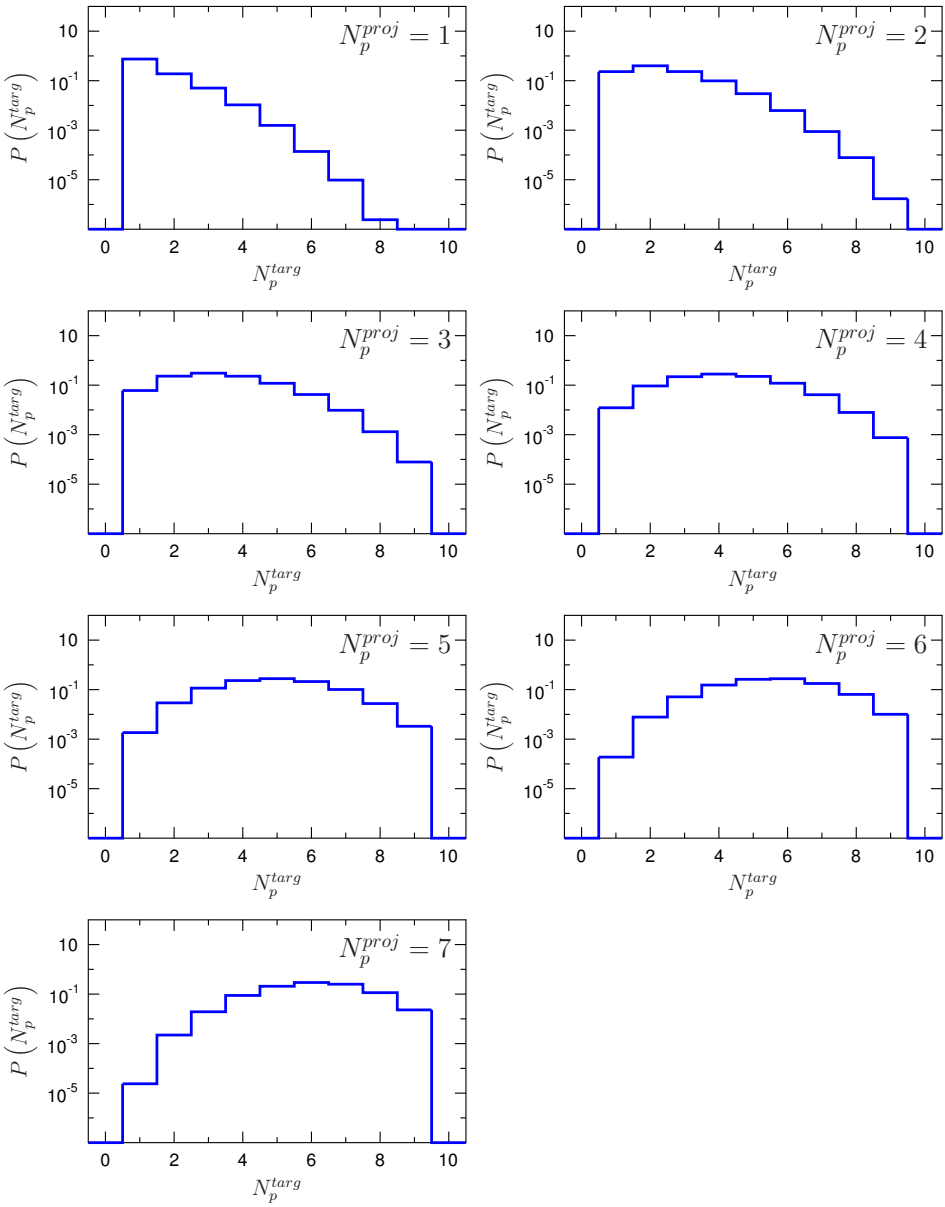

Fig. 14. Probability distributions of target participants for given number of projectile participants in $^{7}\mathrm{Be} + {}^{9}\mathrm{Be}$ production reactions at $\sqrt{s_{NN}} = 16.83$ GeV. NNWP is given by the hard-sphere approximation with expulsion distance $d = 0.9$ fm.

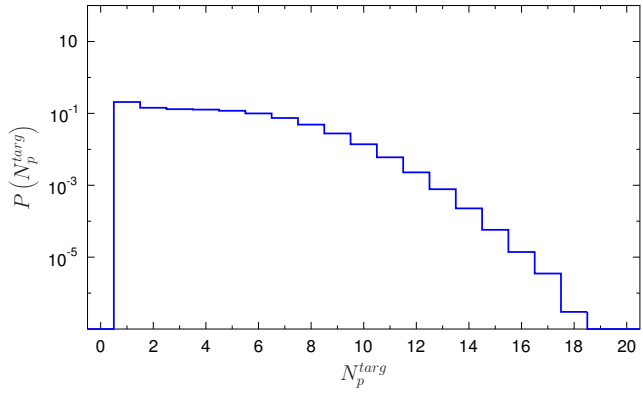

Fig. 15. Probability distribution of target participants in $p + {}^{208}\mathrm{Pb}$ production reactions at $\sqrt{s_{NN}} = 16.83$ GeV. NNWP is given by the hard-sphere approximation with expulsion distance $d = 0.9$ fm.

REFERENCES

[1] J.C. Collins, M.J. Perry, *Phys. Rev. Lett.* **34**, 1353 (1975).

[2] E.V. Shuryak, *Phys. Rep.* **61**, 71 (1980).

[3] M. Gazdzicki, M.I. Gorenstein, *Acta Phys. Pol. B* **30**, 2705 (1999) [arXiv:hep-ph/9803462].

[4] S. Afanasev *et al.* [NA49 Collaboration], *Nucl. Instrum. Methods* **A430**, 210 (1999).

[5] M. Gazdzicki, M. Gorenstein, P. Seyboth, *Acta Phys. Pol. B* **42**, 307 (2011) [arXiv:1006.1765 [hep-ph]].

[6] M.A. Stephanov, K. Rajagopal, E.V. Shuryak, *Phys. Rev.* **D60**, 114028 (1999) [arXiv:hep-ph/9903292].

[7] T. Anticic *et al.* [NA49 Collaboration], *Phys. Rev.* **C81**, 064907 (2010) [arXiv:0912.4198 [nucl-ex]].

[8] T. Anticic *et al.* [NA49 Collaboration], *Phys. Rev.* **C70**, 034902 (2004) [arXiv:hep-ex/0311009].

[9] C. Alt *et al.* [NA49 Collaboration], *Phys. Rev.* **C75**, 064904 (2007) [arXiv:nucl-ex/0612010].

[10] N. Antoniou *et al.* [NA49-future Collaboration], CERN-SPSC-2006-034.

[11] W. Broniowski, M. Rybczynski, P. Bozek, *Comput. Phys. Commun.* **180**, 69 (2009) [arXiv:0710.5731 [nucl-th]]; http://www.ujk.edu.pl/homepages/mryb/GLISSANDO/

[12] R.J. Glauber, in: *Lectures in Theoretical Physics*, W.E. Brittin, L.G. Dunham eds., Interscience, New York, 1959, Vol. 1, p. 315.

[13] A. Bialas, M. Bleszynski, W. Czyz, *Nucl. Phys.* **B111**, 461 (1976).

[14] A. Bialas, M. Bleszynski, W. Czyz, *Acta Phys. Pol. B* **8**, 389 (1977).

[15] M.L. Miller, K. Reygers, S.J. Sanders, P. Steinberg, *Annu. Rev. Nucl. Part. Sci.* **57**, 205 (2007) [arXiv:nucl-ex/0701025].

[16] L.R.B. Elton, *Nuclear Sizes*, Oxford Univ. Press, London, 1961.

[17] H. De Vries, C.W. De Jager, C. De Vries, *At. Data Nucl. Data Tables* **36**, 495 (1987).

[18] K. Hagino, N.W. Lwin, M. Yamagami, *Phys. Rev.* **C74**, 017310 (2006) [arXiv:nucl-th/0604048].

[19] P. Moller, J.R. Nix, W.D. Myers, W.J. Swiatecki, *At. Data Nucl. Data Tables* **59**, 185 (1995) [arXiv:nucl-th/9308022].

[20] W. Broniowski, M. Rybczynski, *Phys. Rev.* **C81**, 064909 (2010) [arXiv:1003.1088 [nucl-th]].

[21] M. Alvioli, H.-J. Drescher, M. Strikman, *Phys. Lett.* **B680**, 225 (2009) [arXiv:0905.2670 [nucl-th]].

[22] See http://www.phys.psu.edu/~malvioli/eventgenerator/

[23] M. Rybczynski, W. Broniowski, *Phys. Part. Nucl. Lett.* **8**, 992 (2011) [arXiv:1012.5607 [nucl-th]].

[24] H. Pi, *Comput. Phys. Commun.* **71**, 173 (1992).

[25] I. Angeli, K.P. Marinova, *At. Data Nucl. Data Tables* **99**, 69 (2013).

[26] N. Abgrall *et al.* [NA61/SHINE Collaboration], *Phys. Rev.* **C84**, 034604 (2011) [arXiv:1102.0983 [hep-ex]].

[27] W. Florkowski, *Phenomenology of Ultra-relativistic Heavy-ion Collisions*, World Scientific, Singapore, 2010.

[28] G. Antchev *et al.*, *Europhys. Lett.* **96**, 21002 (2011) [arXiv:1110.1395 [hep-ex]].

[29] J. Beringer *et al.* [Particle Data Group], *Phys. Rev.* **D86**, 010001 (2012).

[30] M. Rybczynski, W. Broniowski, *Phys. Rev.* **C84**, 064913 (2011) [arXiv:1110.2609 [nucl-th]].

[31] M. Rybczynski, Z. Wlodarczyk, *J. Phys. G: Nucl. Part. Phys.* **41**, 015106 (2014) [arXiv:1307.0636 [nucl-th]].

[32] A. Bialas, A. Bzdak, *Acta Phys. Pol. B* **38**, 159 (2007) [arXiv:hep-ph/0612038].

[33] G. Antchev *et al.* [TOTEM Collaboration], *Europhys. Lett.* **95**, 41001 (2011) [arXiv:1110.1385 [hep-ex]].

[34] G. Antchev *et al.* [TOTEM Collaboration], *Europhys. Lett.* **101**, 21002 (2013).

[35] R. Andrade *et al.*, *Phys. Rev. Lett.* **97**, 202302 (2006) [arXiv:nucl-th/0608067].

[36] A. Bialas, W. Czyz, *Acta Phys. Pol. B* **36**, 905 (2005) [arXiv:hep-ph/0410265].

[37] P. Bozek, W. Broniowski, *Phys. Rev. Lett.* **109**, 062301 (2012)

[arXiv:1204.3580 [nucl-th]].

[38] R.J. Fries, R. Rodriguez, *Nucl. Phys.* **A855**, 424 (2011) [arXiv:1012.3950 [nucl-th]].

[39] R. Brun *et al.*, Root Users Guide 5.16, CERN, 2007.

[40] B.B. Back *et al.* [PHOBOS Collaboration], *Phys. Rev.* **C65**, 031901 (2002) [arXiv:nucl-ex/0105011].

[41] B.B. Back *et al.* [PHOBOS Collaboration], *Phys. Rev.* **C70**, 021902 (2004) [arXiv:nucl-ex/0405027].

[42] M. Gyulassy, D.H. Rischke, B. Zhang, *Nucl. Phys.* **A613**, 397 (1997) [arXiv:nucl-th/9609030].

[43] J. Carvalho, *Nucl. Phys.* **A725**, 269 (2003).

[44] P. Abreu *et al.* [Pierre Auger Collaboration], *Phys. Rev. Lett.* **109**, 062002 (2012) [arXiv:1208.1520 [hep-ex]].

[45] V.P. Konchakovski *et al.*, *Phys. Rev.* **C73**, 034902 (2006) [arXiv:nucl-th/0511083].

[46] I. Weimer, Bachelor Thesis, LMU Munich, 2013.

[47] I. Tanihata *et al.*, *Phys. Rev. Lett.* **55**, 2676 (1985).